OPTO-ELECTRONICS REVIEW **14**(1), 25–32

Uncooled microbolometer detector: recent developments at ULIS

J.L. TISSOT*, C. TROUILLEAU, B. FIEQUE, A. CRASTES, and O. LEGRAS

ULIS, BP 27 – 38113 Veurey-Voroize, France

Uncooled infrared focal plane arrays are being developed for a wide range of thermal imaging applications. Fire-fighting, predictive maintenance, process control and thermography are a few of the industrial applications which could take benefit from uncooled infrared detector. Therefore, to answer these markets, a 35-µm pixel-pitch uncooled IR detector technology has been developed enabling high performance 160×120 and 384×288 arrays production. Besides a wide-band version from uncooled 320×240/45 µm array has been also developed in order to address process control and more precisely industrial furnaces control. The ULIS amorphous silicon technology is well adapted to manufacture low cost detector in mass production. After some brief microbolometer technological background, we present the characterization of 35 µm pixel-pitch detector as well as the wide-band 320×240 infrared focal plane arrays with a pixel pitch of 45 µm.

Keywords: uncooled IRFPA, 2D array, MWIR, LWIR, microbolometer, amorphous silicon.

1. Introduction

Uncooled infrared detectors are now available for various applications. Their simple operating conditions are similar to those of digital CMOS active pixel sensor (APS) used in some digital cameras. They have already shown their potentiality to fulfil many commercial and military applications. One of the key parameters is the low cost achievable with uncooled detectors compared to cooled quantum detectors. Cooled detectors are designed for high performance systems and uncooled detectors are designed for low cost systems and mass production.

This paper describes the advantages of the amorphous silicon technology, the characterization of 35-µm pixel-pitch detectors and the characterization of wide-band 320×240 uncooled detectors. Some mass production results and a short presentation of the next bolometer generation conclude the discussion.

2. Background

The bolometer is composed of a thermometer [1] integrated on a micro-bridge. This micro-bridge is supported by two legs anchored over the silicon substrate by metal studs. This micro-bridge is built on a sacrificial layer which is removed in a final step. The micro-bridge is only 0.1 µm thick of doped amorphous silicon and the distance between the ROIC and the micro-bridge is 2.5 µm (Fig. 1). This vacuum gap works as a quarter wavelength cavity, which sets the detector spectral response maximum at a wavelength close to 10 µm. However, the measured response is still substantial in the 3–5 µm range as shown in the following paragraphs.

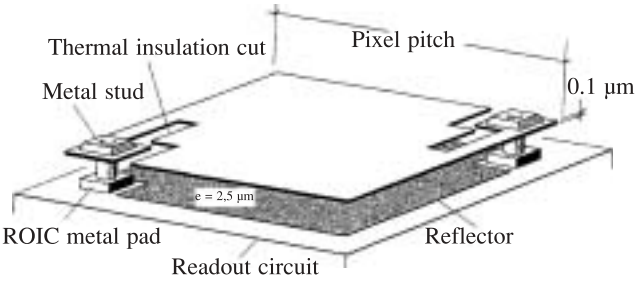

Fig. 1. Bolometer pixel structure.

Besides its silicon technology compatibility, amorphous silicon presents many other advantages. First, it enables the manufacturing of very thin suspended membranes (1000 Å) combined with short leg lengths resulting in high fill factor and high mechanical strength structures that could sustain high vibration rates and high mechanical shocks. This reduced mechanical susceptibility to vibration or shock solicitation is obviously important for many military as well as commercial applications. Secondly, the very thin thermally isolated suspended membrane, along with the low thermal mass of silicon, results in a very low pixel thermal time constant (approx. 4 ms for 45 µm pixel pitch and 7 ms for 35 µm and 25 µm pixel-pitch). Moreover, this simple technology leads to high manufacturing yield and therefore low manufacturing cost.

3. 35-µm pixel-pitch uncooled IRFPA

For enabling the design of 35-µm pixel pitch devices while keeping high performance, CEA/LETI has defined new process flow and pixel design with advanced design rules,

*e-mail: jl.tissot@ulis-ir.com

The paper presented there appears in *Infrared Photoelectronics*, edited by Antoni Rogalski, Eustace L. Dereniak, Fiodor F. Sizov, Proc. SPIE Vol. 5957, 59570M (2005).

to improve the thermal insulation from 1.4×10^7 K/W up to 4.2×10^7 K/W. Moreover, the pixel structure still uses a one level structure, the manufacture of which is much easier than double deck structures. In order to limit the low frequency noise, a specific design of the pixel has been developed, which essentially maximizes the sensitive material volume defining the electrical resistance. Namely, the membrane thickness has been adjusted on the basis of 7 ms thermal time constant (Rth.Cth), still compatible with 60 Hz video frame rate. The resulting mean *NETD* (f/1, 300 K, 60 Hz) has been dropped to 30 mK. The characteristics of this 2nd generation process flow are summarized in the following table for a 35×35 μm¸ pixel pitch.

Table 1. 35-μm pixel size parameters.

R_{th} (K/W)	τ_{th} (ms)	*NETD* (mK)	Fill factor
4.2×10^7	7	< 30	> 80%

This 2nd generation technology enables the manufacturing of products based on 35-μm pixel size and leads to dramatic improvement in performance and cost.

3.1. ROIC design

The two CMOS readout integrated circuits (384×288 and 160×120) have a similar structure to the 45 μm 320×240 focal plane array. The pixels are pulse-biased row by row. Figure 2 shows the synoptic of the signal processing from one pixel to the video signal output. A blind bolometer suppresses the background current. Then, the signal is integrated in a capacitance trans-impedance amplifier. Afterwards, during the next row time, this integrated signal is held, multiplexed, and finally amplified. Figure 3 shows that the skimming, integration and sample and hold functions are located at one end of each column.

Compared to the 45-μm product, several on-chip features have been added to simplify the use of these new

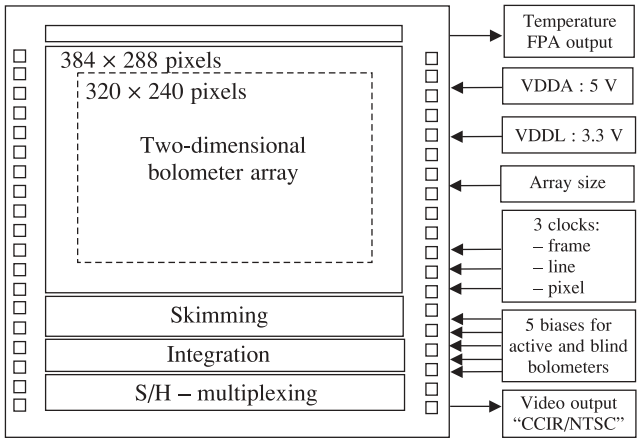

Fig. 3. 320×240/384×288 ROIC schematic.

IRFPAs. These new components take advantage of the 3.3 V/5 V voltage supplied by the 0.5 μm – 5 V CMOS technology. Even if the three clocks are pulsed in 3.3 V, the analogue part, which is supplied in 5 V, enables to get a dynamic range from 0.4 to 3.2 V. This ensures a wider dynamic range with a low *NETD* and takes benefit for TEC-less use. These two ROICs have been designed to consume less than 70 mW for the 160×120 array and less than 130 mW for the 384×288 array.

An on-chip biases module, based on a band-gap structure, generates most of the voltage and current biases. The outputs of this module are stabilized against temperature fluctuations (< 100 ppm/°C) and leads to a high noise rejection on analogue biases. This module and the 3.3 V clocks provide a simple electrical interface requiring only three 3.3 V clocks and five biases. Moreover, the internal data processing has been designed in order to deliver a video compliant with CCIR and NTSC formats.

An on-chip thermometer, based on a p/n silicon junction with a buffer to prevent any ROIC parasitic coupling,

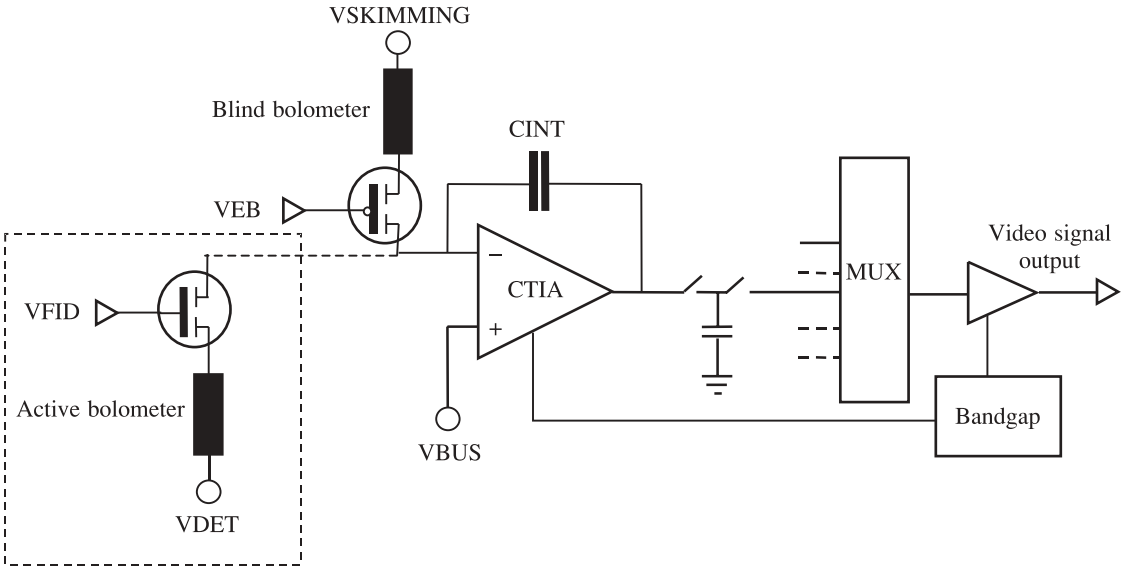

Fig. 2. Synoptic of the pixel readout architecture.

Fig. 4. UL 03 08 1 – 384×288, 35-µm pixel pitch.

has been implemented in the readout circuit to deliver a voltage VTEMP that follows ROIC temperature variation. For TEC-less operation, VTEMP output can be used to adjust the different operating points.

Finally, the wider array ROIC provides two different array sizes: 320×240 and 384×288 formats by applying 3.3 V or ground on the "SIZE" input pad.

3.2. Packaging

Two new flat packages have been developed for the two arrays 384×288 (3202×40) and 160×120 with 35-µm pixel pitch. These packages (Figs. 5 and 6) are based on available technologies widely developed for the packaging of mass produced electronic devices.

The lead frames enable electronic board integration like it is for standard CMS devices, insuring high electrical contact reliability in tough and demanding environmental applications such as military operations, fire fighting, process control or predictive maintenance.

The package of the UL 02 05 1 (160×120/35 µm pixel pitch) is a standard package often used for the telecom market. Only the processes used to assemble the thermoelectric cooler, the die and the window housing have been adapted to take into account the required lifetime under vacuum.

Conversely, the package of the UL 03 04 1 (384×288) is designed in house. It is a lead-free metal package assembled with high reliability ceramic feed through technology.

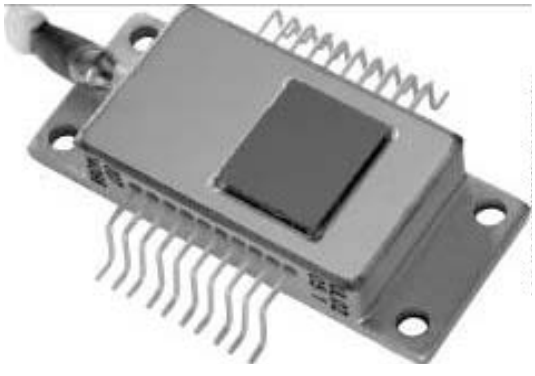

Fig. 5. UL 02 05 1 – 160×120, 35-µm pixel pitch.

Fig. 6. UL 03 04 1 – 384×288 (320×240), 35-µm pixel pitch.

The package base plate is composed of a highly heat conductive material allowing efficient thermal transfer either through the back or the front of the package.

The distance between FPA and external window side is 1.32 mm enabling the possibility to use short back working-distance optics. Additionally, for both detectors UL 03 08 1 and UL 03 04 1, the optical centre is the same for the two array formats 384×288 or 320×240. This package developed for wide bolometer arrays, is compatible with the 640×480 microbolometer FPAs with 25-µm pitch pixels currently under development at ULIS.

3.3. Electro-optical tests

As characteristics of UL 02 05 1 have already been presented [2,3], this part focuses only on the tests of the UL 03 04 1 and UL 03 08 1 full size 384×288. All electrical and electro-optical tests are defined and carried out with f/1 optical aperture, a background temperature at 293 K and a FPA controlled at 303 K. The excellent linearity above 99% on the total electrical range (0.4–3.2 V) allowed all the tests at 60 Hz frame rate and with a 6.4 MHz master clock. Moreover, all the presented tests correspond to a typical polarization and a 59.3 µs integration time. Figure 7 shows the histogram and also a map of an output DC level for a detector presented in front of a 293 K blackbody without any correction. The electrical dynamic range extends from 0.4 V to 3.2 V.

Very few bad pixels are located on this map. The knowledge and control of bolometer technology acquired over the last years allows the production of 35-µm bolometer arrays with a pixel-operability much higher than 99.5%. The responsivity (7.2 mV/K, σ 1.1%) is measured between two blackbodies at 293 K and 308 K. Therefore, by considering Planck's law, if we associate the available electrical dynamic range (0.4–3.2 V) presented in Fig. 7 and the mean value of the responsivity, the temperature dynamic range could be higher than 200°C without any pixel saturation before correction or calibration. Associated with a mean rms noise of 310 µV, presented in Fig. 8, these

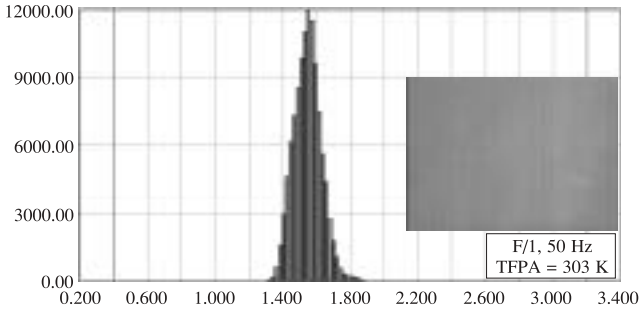

Fig. 7. Output raw DC level distribution and map.

35-µm pixel pitch detectors achieve a mean *NETD* of 43 mK for f/1, 50 Hz and a 303 K background.

All these results obtained with this wide FPA confirm the characteristics on the smaller array 160×120/35 µm pixel pitch. Moreover, *NETD* as low as 27 mK has already been demonstrated under the same conditions with reduced scene temperature dynamic range. The detector operating point could be tuned in line with the application. It is a trade off between *NETD* performance and the available scene temperature dynamic range. Number of applications such as process control, need a high temperature dynamic range while others like medical applications, require a better *NETD* with a dynamic range of a few degrees.

Both the spatial and temporal *NETD* of a UL 03 08 1 are presented in Fig. 8. We observe the characteristic "W" shape of the spatial *NETD* with the two minima at 20°C and 40°C. These points correspond to the two points of gain and offset calibration. Within this range, the spatial *NETD* is always below the temporal *NETD* to ensure that the spatial patterns are not distinguished from the temporal noise on the image. By combining a mean temporal *NETD* of around 43 mK and the improved power supply rejection ratio, the images of the 384×288 are sharply contrasted and present a high quality resolution.

3.4. Mass production feasibility

The following bar-chart offers the distribution of the standard deviation of the responsivity on more than 3000 U 02 05 1 issued during 2004.

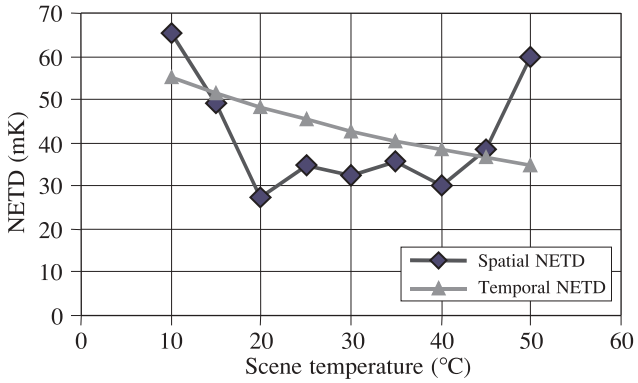

Fig. 8. Spatial and temporal *NETD* (TPFA = 30°C).

Table 2. Summary of typical characteristics of UL 03 08 1.

Array configuration	384×288/320×240
Pitch size	35×35 µm
Nominal operating temperature	30°C
Spectral response	8–14 µm
Typical responsivity	7.2 mV/K
Typical noise	310 µVrms
Typical *NETD* @ f/1	43 mK
Operability	> 99.5%
Thermal time constant	< 7 ms
Spatial *NETD*	< temporal *NETD*
Power dissipation	130 mW
Typical frame rate	60 Hz
Output video	CCIR–NTSC compatible
NETD×time constant	300E-6

This low and constant standard deviation of 1.4% demonstrates the excellent homogeneity for a large number of detectors. Also, first results on the 384×288 arrays show the same productiveness. The excellent yield and the mastering of the 35-µm technology allow ULIS to produce highly uniform detectors.

4. New developments

The development of the 3rd generation has been under progress at CEA/LETI for few years and a first 320×240 arrays has been developed with a pixel pitch of 25 µm. The pixel architecture developed for this small pixel pitch is still based on a one level structure while pushing the pixel design improvement to some further limits. This new architecture leads to obtain high performance in conjunction with small thermal time constants. The first prototype shows a mean *NETD* of 75 mK (f/1, 60 Hz, 300 K) with 6 ms as thermal time constant. This very low thermal time constant leaves a large margin to increase the performance of this new detector further. These results demonstrate that

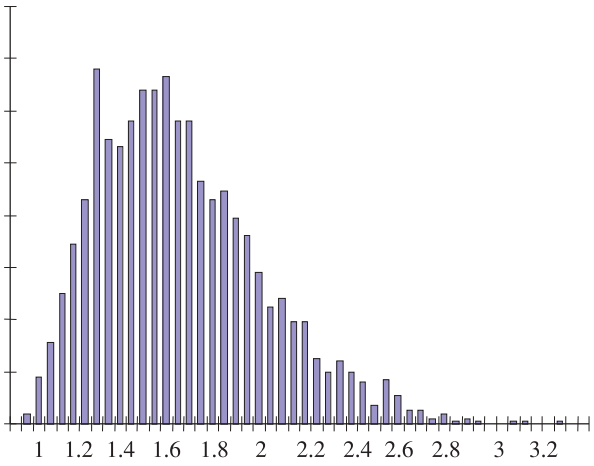

Fig. 9. Distribution of responsivity standard deviation (%) on more than 3000 UL 02 05 1.

amorphous silicon may compete with other developments even at reduced pitches, while maintaining a small thermal time constant with a very simple process [4].

Based on this first result, a 640×480 array is currently developed and will be mass produced from 2005 as well as a 320×240 for automotive application.

5. Wide-band 320×240 uncooled IRFPA

In theory, a thermal bolometer made from a resistively coupled thin film membrane shows a flat response across the entire spectrum. However, in order to maximize the response in the LWIR, these semi-transparent thin film structures are traditionally built with a quarter wave optical cavity under the membrane. This cavity increases the absorption efficiency in the LWIR by re-capturing some of the missed LWIR flux reflected back by an aluminium reflector. The peak absorption wavelength λ_p dictated by the optical cavity is given by Eq. (1) where n is the index of refraction of the transmission media in the cavity (vacuum), e is the cavity depth, and k is the resonant order

$$ne = \frac{(2k+1)\lambda_p}{4}. \quad (1)$$

As a consequence, for n = 1 (vacuum), e ~2.5 μm, and k = 0, λ_p = 10 μm which corresponds to the standard ULIS microbolometer array product in the LWIR. For k = 1, λ_p = 3.33 μm. Therefore, the standard ULIS microbolometer pixel structure should exhibit increased absorption factor in the MWIR, although not as high as that in the LWIR.

One can evaluate the result of such quarter-wave cavity, in Fig. 10, where the microbolometer response and the contribution of this cavity are described. In this figure, we can see both the measured microbolometer response and the theoretical quarter-wave response for a 2.5-μm cavity. For the theoretical curve, the response is calculated for an infinite pixel and all process layers are taken into account. In this case, the fill factor is considered as 100%. For the other curve, the measurement method of the spectral response is described in the next paragraph.

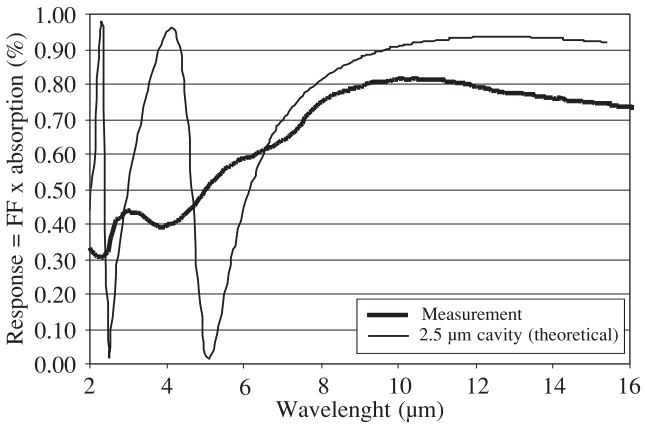

Fig. 10. Quarter-wave cavity (theoretical and measured) spectrum.

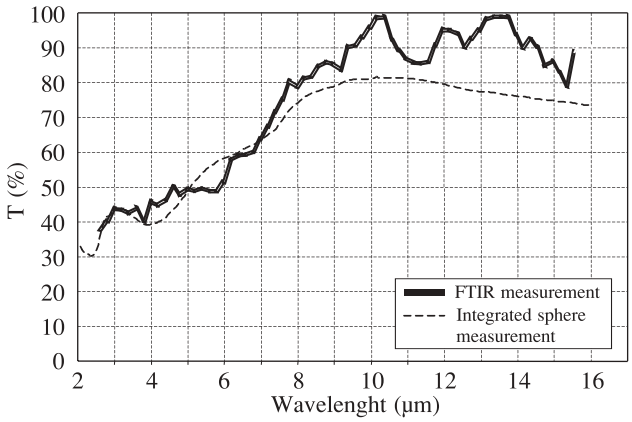

Fig. 11. Microbolometer chip spectral response measurement.

5.1. Microbolometer chip spectral response

As it can be seen in Fig. 11, the spectral response of the microbolometer is efficient in the 3–5 μm band. Two different methods have been used to measure the microbolometer response. The first one corresponds to a method which takes the fill factor into account. The response is indirectly measured, with an IR spectrometer equipped with an integration sphere. A large beam (~5 mm diameter) is shed on the array and the total reflected, diffracted or diffused back flux is detected, and normalized against the spectral reflectivity of a reference mirror. We assume the quantity (1–R) to be closely representative of the effective spectral absorption, and hence of the response. The other one is the microbolometer response of one pixel measured with an FTIR bench (Fourier transform infrared).

Characterization elements explain the differences between the two results shown in Fig. 11. First, as noticed before, the fill factor is not taken into account in the FTIR method because only one pixel is sampled in this electrical measurement. Moreover, in this measure, the results are normalized to the maximum value, and therefore, the detector window transmission is de-correlated from the rough FTIR measurement. Despite these differences, the rough curves profiles are the same.

5.2. Filters

For wide-band prototype development, a specific 3–5 μm and 8–16 μm ranges detector window has been used. Its transmission is shown in Fig. 12. An added sapphire filter, placed on the optical path, has also been used (Fig. 13) in order to cut-off the atmospheric transmission beyond 5 μm.

5.3. Responsivity evaluation

We assessed the responsivity in the MWIR range by multiplying the microbolometer responsivity presented in Fig. 11 by the window prototype transmission shown in Fig. 12. This result is given in Fig. 14. On the same graph, one can see the calculated luminance for a black body at 450°C and 650°C.

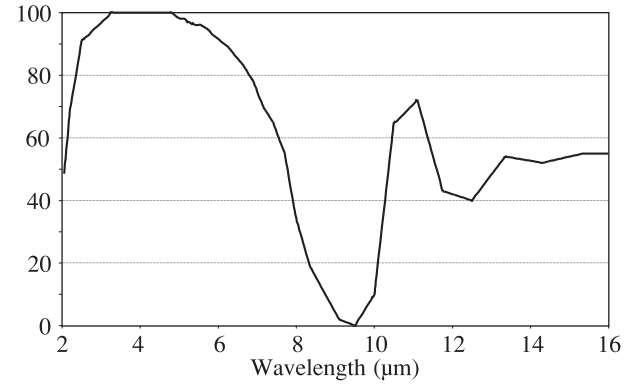

Fig. 12. Wide-band window prototype transmission.

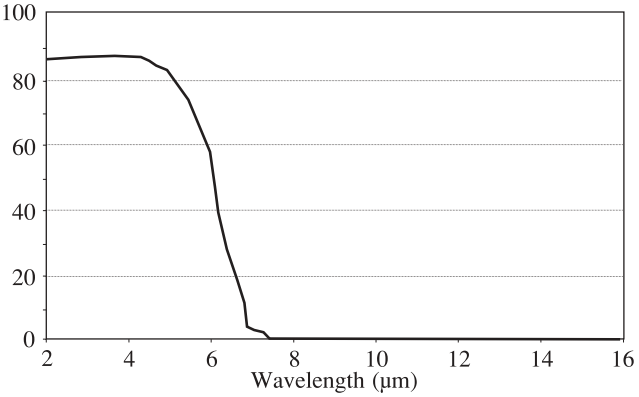

Fig. 13. Sapphire filter transmission.

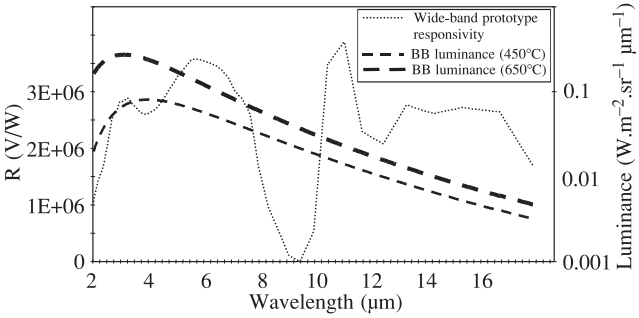

Fig. 14. Microbolometer responsivity over the waveband.

What is very important to notice, is that, even if the microbolometer response in the 3 to 5 μm range is half the response in the 8–14 μm range, the flux coming from a blackbody at 450°C or 650°C is roughly ten times higher in the 3–5 μm range than in the 8–14 μm range. In order to compare the standard 8–12 μm detector and the wide-band detector prototype, we define a factor of merit which is a signal difference ΔV ratio, or responsivity ratio. This ratio allow us to compare a signal difference for a given temperature T and a given wavelength range to the signal difference calculated for 30°C in the 8–12 μm wavelength range.

Following Planck's law, one can determine this signal difference ΔV we can reach, and the factor of merit FOM

$$\Delta V = R_{mean} \int \frac{\partial L}{\partial \lambda} d\lambda A_{\text{det}} \Omega \qquad (2)$$

$$FOM = \frac{\Delta V_{\lambda low - \lambda high}(T)}{\Delta V_{8-12\,\mu m}(30^\circ C)} \qquad (3)$$

Where A_{det} is the sensitive bolometer membrane surface and Ω is the solid angle $\Omega = \pi / 4f^2$ calculated with the f number. As a result, we can estimate a sensitivity comparison (FOM) for different temperatures and wavelength ranges. Table 3 provides these results.

Table 3. Calculated relative response versus wavelength ranges.

Detector	λ_{low} (μm)	λ_{high} (μm)	T_{BB} (°C)	Relative response
Standard LWIR 320×240/45 μm	8	12	30	1
Standard LWIR 320×240/45 μm	8	12	450	4
Wide-band 320×240/45 μm	3	5	450	6.6
Wide-band 320×240/45 μm	3.5	5	450	4.8
Wide-band 320×240/45 μm	3.7	4.8	450	3.4

Table 3 shows that the relative response is more than six time higher for a 450°C scene temperature with the wide-band prototype detector (in the 3–5 μm range) than with the LWIR standard detector (in the 8–12 μm range) for a 30°C scene temperature. Other wavelength range relative responses are presented in order to fit specific applications.

5.4. Electro optical characterization

In order to evaluate the performances in the 3–5 μm wave band range, a high temperature cavity blackbody has been used. We placed a diaphragm in the optic path to fix the field of view. The f number resulting from the limiting diaphragm amounts to 9.54. Figure 15 shows a schematic of the experimental setup, and Fig. 16 is a plot of the DC output level for different blackbody temperature. We also have carried out measurements with a sapphire filter in order to cutoff the atmospheric transmission beyond 5 μm.

We calculated the derivative against temperature of the previous results. This leads to the responsivity R presented below. The previous results have been obtained with f/9.54. In order to compare these results with classical optical aperture we extrapolate the results at f/1. This extrapolation is

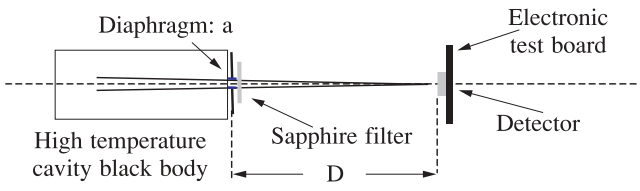

Fig. 15. Experimental setup.

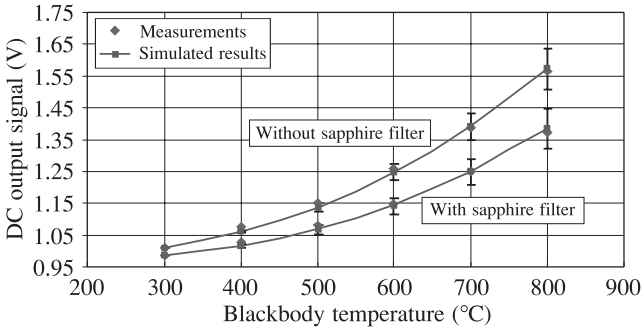

Fig. 16. DC output signal versus blackbody temperature (@*f*/9.54).

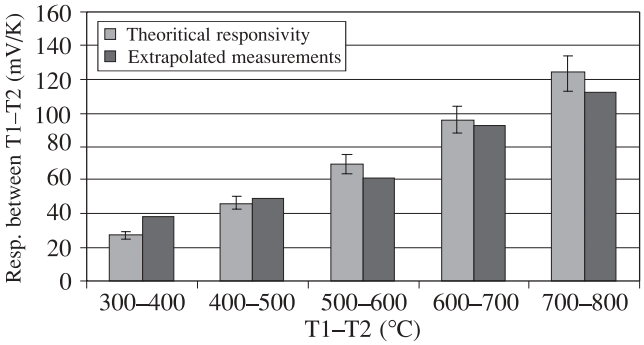

Fig. 17. Responsivity with sapphire filter for different ranges of high temperatures (@*f*/1).

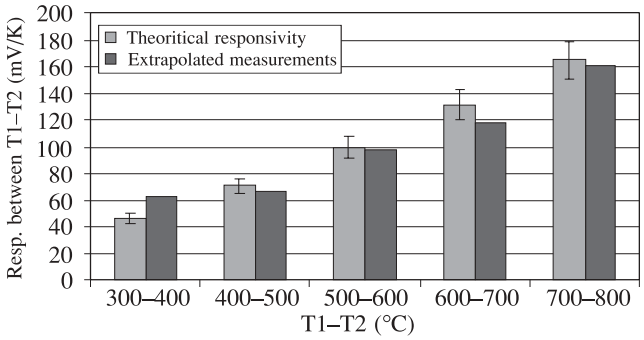

Fig. 18. Responsivity without sapphire filter for different ranges of high temperatures (@*f*/1).

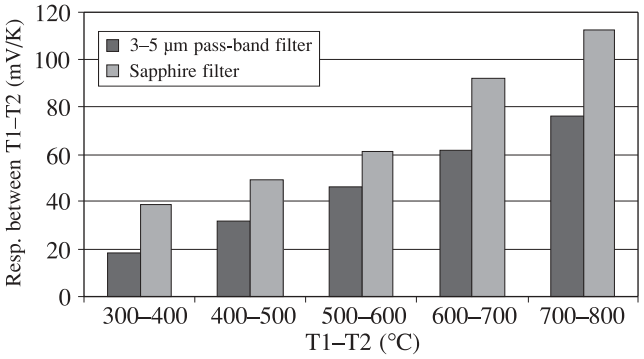

Fig. 19. Responsivity with sapphire filter and with 3–5 µm filter for different high temperatures ranges (@f/1).

obtained by using the relation $R_1/\Omega_1 = R_1/\Omega_2$ where R_1 and R_2 are the responsivity associated with the Ω_1 and Ω_2 solid angles. Ω is related to the f number, by the formula $\Omega = \pi/4f^2$. The extrapolated responsivity can be seen in Figs. 17 and 18.

We can fit any specific filter onto a camera, in order to match the detector with a given application. We tried to simulate what could be expected with the wide-band prototype detector provided with a perfect 3–5 µm band pass (with 100% transmission between 3 and 5 µm, and 0 outside that range).

Table 4 summarizes all the results and points out that the responsivity will be close to 45 mV/K @*f*/1 for 450°C temperature scene and 30 mV/K with additional 3–5 µm filter.

Table 4. Results summary for *f*/1.

	With sapphire filter	Without sapphire filter	3–5 µm band pass filter. Extrapolation result
Responsivity between 400°C and 500°C	49 mV/K	66 mV/K	31 mV/K

For some applications, we have to be able to detect a hot spot in a background environment at 20°C, for example in aerial observation such as fire detection from satellites [5]. In this case, the signal to noise ratio is very high because the response is measured between 20°C and high temperature (i.e., 450°C).

The next table summarizes the wide-band detector prototype parameters and performances.

Different pictures have been taken with both detector in both ranges (3–5 µm and 8–12 µm). We can see differences of temperature on the soldering iron with the wide-band detector whereas with the 8–12 µm detector, the signal saturate on the iron (Fig. 20).

Table 5. Detector summary (values @*f*/1).

	Range	
	LWIR – 30°C	MWIR – 450°C
Responsivity	5 mV/K	45 mV/K
Array size	320×240	
Pixel pitch	45 µm	
Operability	> 99.5%	
Pin out	Fully compatible with UL 01 01 1 electronics board	

6. Improvement in progress

The current filter of the wide-band prototype window allow the detector to have a sufficient responsivity both in the 3–5 µm and in the 8–12 µm wave band. But the drawback of this filter is the cut-off at 9.5 µm and its poor transmission in the region close to 7 µm to 8 µm which could be a disadvantage for some gas detection. An improved win-

3–5 μm (wide-band detector prototype)

8–12 μm (LWIR detector)

Fig. 20. Soldering iron (temperature 450°C).

dow with a continuous high transmission in a spectral range from 3 to 16 μm is under test. It leads to the improved spectral response shown in Fig. 21 which is to be compared with the first prototype spectral response shown in Fig. 14.

7. Conclusions

Developments of amorphous silicon microbolometer technology have been focusing on the improvement of their sensitivity, enabling the possibility of manufacturing high performance devices with small pixel pitch, at a low cost. The 320×240/384×288 and 160×120 with 35-μm pixel pitch arrays have demonstrated high uniform performance and very low thermal time constant which open the field to new applications. The tuning of these focal plane arrays enables ULIS to match many applications from high dynamic range for industrial controls or small dynamic range and low NETD like medical applications. Technology development is in progress to enable the production of a new gen-

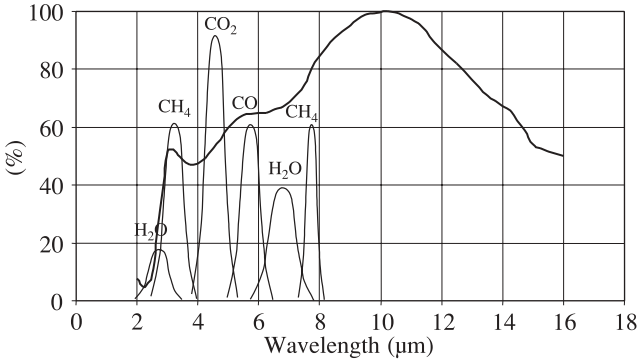

Fig. 21. Spectral response of the improved detector under development in comparison with different gas detection wavelength.

eration 25-μm pixel-pitch detectors in 640×480, 384×288, and 160×120 formats.

Besides, new detectors with wide-band sensitivity based on standard 320×240/45 μm pixel pitch detector have been demonstrated. The fields of application are in industrial processes, thermography, gas detection and furnace control or fire detection.

Acknowledgments

The authors would like to thank LETI LIR Uncooled detectors Teams and ULIS personnel who develop and produce uncooled infrared microbolometer detectors. We also thank Sofradir staff for their contribution and their support.

Reference

1. C. Vedel, J.L. Martin, J.L. Ouvrier-Buffet, J.L. Tissot, M. Vilain, and J.J. Yon, "Amorphous silicon based uncooled microbolometer IRFPA", *Proc. SPIE* **3698**, 276–283 (1999).
2. C. Trouilleau, A. Crastes, J.L. Tissot, J.P. Chatard, and S. Tinnes, "Amorphous silicon based uncooled microbolometer IRFPA", *Proc. SPIE* **5251**, 272–279 (2003).
3. J.L. Tissot, M. Vilain, A. Crastes , S. Tinnes, A. Larre, O. Legras, and J.J. Yon "Uncooled IRFPA with high performance and low thermal time constant", *Proc. SPIE* **5612**, 72–77 (2004).
4. J.J. Yon, A. Astier, S. Bisotto, G. Chamings, A. Durand, J.L. Martin, E. Mottin, J.L. Ouvrier-Buffet, and J.L. Tissot, "First demonstration of 25-μm pitch uncooled amorphous silicon microbolometer IRFPA at LETI-LIR", *SPIE Proc.* **5783**, 432–440 (2005).
5. B.D. Oelrich, A. Crastes, C.I. Underwood, and S. Mackin, "A low-cost mid-wave IR microsatellite image concept based on uncooled technology", *Proc. SPIE* **5570**, 209–217 (2004).

